Spatiotemporal variations of total suspended matter (TSM) in the Pearl River estuary using MERIS full-resolution (FR) level-2 TSM product

Article *in* Marine and Freshwater Research · January 2019

DOI: 10.1071/MF18111

CITATIONS
0

READS
30

5 authors, including:

Feng Gao
Shanxi University of Finance and Economics
6 PUBLICATIONS **5** CITATIONS
SEE PROFILE

Yunpeng Wang
Chinese Academy of Sciences
122 PUBLICATIONS **1,293** CITATIONS
SEE PROFILE

Chao Xu
Chinese Academy of Sciences
7 PUBLICATIONS **4** CITATIONS
SEE PROFILE

CSIRO PUBLISHING

Marine and Freshwater Research, 2019, **70**, 1065–1077
https://doi.org/10.1071/MF18111

Spatiotemporal variations of total suspended matter (TSM) in the Pearl River estuary using MERIS full-resolution (FR) level-2 TSM product

Feng Gao[A,B], *Yunpeng Wang*[A,D], *Xinyi Hu*[A,B], *Chao Xu*[A,B] *and Ned Horning*[C]

[A]State Key Laboratory of Organic Geochemistry, Guangzhou Institute of Geochemistry, Chinese Academy of Sciences, Guangzhou, 510640, PR China.
[B]University of Chinese Academy of Sciences, Beijing, 100049, PR China.
[C]American Museum of Natural History Center for Biodiversity and Conservation, Central Park West at 79th Street, New York, NY 10024, USA.
[D]Corresponding author. Email: wangyp@gig.ac.cn

Abstract. In this study, we first use self-organising map (SOM) and medium-resolution imaging spectrometer (MERIS) full-resolution (FR) level-2 total suspended matter (TSM) product to identify spatial-distribution patterns of TSM concentration in the Pearl River estuary. Second, the spatial and temporal variation of TSM concentration in the Pearl River estuary was investigated using 9-year (2003–2011) MERIS FR level-2 TSM products. The spatial-distribution patterns of TSM concentration identified by SOM in the Pearl River estuary showed that there are high values in west and north and low values in east and south. On the basis of the analysis of the sample points randomly extracted from the Pearl River estuary, the results showed that the spatial variation of TSM in eight gates varied greatly, and the Lingdingyang Bay from Humen to offshore waters (i.e. Xitan, Zhongtan and Dongtan) presents a decreasing trend. Moreover, extreme climate events (e.g. EI Niño and La Niña) may have a great effect on spatial and temporal variation of TSM concentration in the Pearl River estuary. These results could provide a new insight for a better understanding of the dynamics of TSM concentration in the Pearl River estuary and the effect of soil- and water-conservation measures in the upstream of Pearl River.

Additional keywords: EI Niño and La Niña, precipitation, SOM, spatial and temporal variation.

Received 21 March 2018, accepted 12 December 2018, published online 18 February 2019

Introduction

Surface water quality is a matter of serious concern today, in which total suspended (TSM) matter plays an important role in ecology, geomorphology and turbidity in estuarine and coastal waters (Li *et al.* 2012; Varol *et al.* 2012; Robert *et al.* 2016). TSM dynamics in estuarine are determined by a complex natural process and anthropogenic activities (Suif *et al.* 2016), which are strongly related, for example, to the urbanisation, agriculture, deforestation, climate change and construction of water conservancy project. The main component of TSM is suspended sediment, which is easily changed with time, owing to many factors, such as water discharge conditions, winds, tides as well as human activities (Rodríguez-Blanco *et al.* 2010; Li *et al.* 2012; Chen *et al.* 2015; Sun *et al.* 2016). In recent decades, many researchers have focused on the retrieval of TSM concentration by combining remote-sensing data and field measurements of TSM in the Pearl River estuary (PRE; Liu *et al.* 2009; Xi and Zhang 2011; Xing *et al.* 2013; Zhu *et al.* 2015). However, few studies have focused on the study of spatial and temporal variations of TSM from long-term satellite-derived TSM datasets and their impact factors.

The Pearl River delta (PRD) is one of the most developed areas in China, owing to implementation of China's open-door and reform policies since the 1980s, and at least 8636 reservoirs had been constructed in the Pearl River watershed by the late 1990s. The hydrological regime of the Pearl River basin has been substantially changed by this intensive human activity, and the Pearl River has become one of the most highly affected rivers in the world (Wu *et al.* 2016). As a consequence, the natural sediment transport regime in the Pearl River delta has been altered as a result of dam construction and soil conservation (Wu *et al.* 2016). In addition, the urbanisation level of the PRD increased from 29.6% in 1982 to 71.4% in 2000 (Ouyang *et al.* 2006). These changes will have a great effect on the variability of water-quality parameters because of large differences in sediment load and water discharge, especially for the TSM concentration in the PRE.

Satellite remote sensing, as an effective method for retrieving TSM and other relevant water-quality parameters, has been widely used to retrieve and study the dynamics of the TSM concentration in coastal and estuary waters in the world (Miller and McKee 2004; Chen *et al.* 2006, 2016; Onderka and

Pekarova 2008; Liu *et al.* 2010; Mao *et al.* 2012; Yu *et al.* 2012; Cheng *et al.* 2013; Downing-Kunz and Schoellhamer 2013; Duan *et al.* 2013; Restrepo *et al.* 2016; Liang *et al.* 2017). The medium-resolution imaging spectrometer (MERIS) is the first ocean colour sensor launched by the European Space Agency (ESA; Kratzer *et al.* 2008). It provides imagery with moderate spatial resolution of 300 m and 15 spectral bands in the visible–NIR regions, which facilitates its potential use in coastal and estuary waters (Le *et al.* 2016). The standard product for Case-2 waters produced by ESA is the MERIS Case 2-Regional Processor (C2R; Doerffer and Schiller 2007; González Vilas *et al.* 2011). This algorithm uses the logarithm of the remote-sensing reflectance above the surface of 8 of the 15 MERIS bands after atmospheric correction and neural network techniques, so as to determine three inherent optical properties (IOPs) of the water (absorption of pigments, yellow substance and scattering of all particles; Doerffer and Schiller 2007; Kratzer *et al.* 2008; González Vilas *et al.* 2011). The three Case-2 water products of MERIS (chlorophyll *a*, total suspended matter and yellow-substance absorption) were derived from the three IOPs (Kratzer *et al.* 2008).

In the past few years, a great number of work has been conducted on validating MERIS products in coastal and estuary waters (Schroeder *et al.* 2007; Sørensen *et al.* 2007; Alikas and Reinart 2008; Liu *et al.* 2009; Shen *et al.* 2010). Liu *et al.* (2009) explored the MERIS data for the evaluation of TSM concentration in the PRE, by using field remote-sensing reflectance and *in situ* measurements of TSM. The results demonstrated that a high correlation coefficient was obtained between the estimated TSM concentration and MERIS full-resolution (FR) level-2 TSM products. Nine years of MERIS FR level-2 archive data (2003–2011) were available and chosen for the study of spatial and temporal variations of TSM concentration in the PRE during the period from 2003 to 2011.

Therefore, the specific objectives of the study were to (1) identify the spatial-distribution patterns of TSM concentration in the PRE from 2003 to 2011, (2) study the spatial and temporal variations of TSM concentration in the PRE from 2003 to 2011 and (3) analyse the factors that influence the variations of TSM concentration.

Materials and methods

Study area and sample points

The PRE is a subtropical estuary embedded in the southern coast of China (Fig. 1), which is the estuary of Pearl River network. The Pearl River is the 13th largest river in the world and the 2nd largest river in China in terms of freshwater discharge (Lu and Gan 2015). The physical and biogeochemical processes in the PRE show strong seasonality because of the south-west monsoon in summer and north-east monsoon in winter and that the discharge of Pearl River (PR) mainly depends on the amount of rainfall (Lu and Gan 2015; Wang *et al.* 2018). Approximately 80% of the discharge from the PR happens during the wet season from April to September (Zhai *et al.* 2005; Lu and Gan 2015). In addition, variability induced by tidal activities also have a great influence on the seasonal processes (Lu and Gan 2015). The annual mean surface runoff is 3.26×10^8 m^3 and sediment load is $\sim 7.53 \times 10^7$ Mg year^{-1}, on average. In the past few decades, the water discharge and sediment load of the Pearl River have experienced a decreased trend (Dai *et al.* 2008; Wu *et al.* 2012, 2014, 2016).

The Pearl River has three major tributaries, Xijiang (the west river), Beijiang (the north river) and Dongjiang (the east river). The water discharge of Beijiang and Dongjiang is small, only contributing 22.8% of the total discharge in the PR, whereas the Xijiang accounts for 68.5% (Wu *et al.* 2014). The runoffs of the three major tributaries and other small water channels are all discharged into the South China Sea (SCS) via eight major outlets (Fig. 1). These outlets include Humen, Jiaomen, Hongqili, Hengmen, Modaomen, Jitimen, Hutiaomen and Yamen. Four eastern outlets (namely Humen, Jiaomen, Hongqili and Hengmen) mainly collect the runoff from the Dongjiang and Beijiang and some other small rivers, as well as from a portion of the Xijiang. The discharges from these four eastern outlets pour into the large subestuary in the PRD, namely Lingdingyang Bay (dashed box in Fig. 1). The PRE refers to the Lingdingyang Bay and other outer water. For the ease of analysis and discussion, we divide the Lingdingyang Bay into three parts, namely Xitan, Zhongtan and Dongtan (dashed box in Fig. 1). Five sample points in Xitan (W1, W2, W3, W4 and W5), six sample points in Zhongtan (M1, M2, M3, M4, M5 and M6) and six sample points in Dongtan (E1, E2, E3, E4, E5 and E6) were selected for studying spatial and temporal variation of the TSM concentration in the PRE.

Image acquisition and pre-processing

MERIS FR level-2 TSM product, produced by the European Space Agency's sensor MERIS on the ENVISAT-1 satellite, was used in this study. MERIS has an improved spatial resolution of 300 m, with a re-visit period of 1–3 days (latitude dependent). In addition, MERIS also has nine narrow spectral bands in the range of 412–708 nm. The logarithm of the remote-sensing reflectance above the surface of 8 of the 15 MERIS bands after atmospheric correction was used to retrieve MERIS water products by using a neural network (NN; Kratzer *et al.* 2008). The eight bands used for deriving the level-2 products are centred at 412, 442, 490, 510, 560, 620, 665 and 708 nm. In addition, solar and viewing zeniths, as well as azimuth difference are required to input into the NN algorithm. The output of NN is the logarithm of the following three IOPs: pigment absorption at 442 nm, the summed-up absorption of yellow substance and the scattering coefficient of all suspended particulate matter at 442 nm (Kratzer *et al.* 2008). The IOPs are then used to derive the concentration of chlorophyll *a* and TSM (dry weight), as well as yellow-substance absorption, which form the three Case-2 water products of MERIS. MERIS FR level-2 TSM images were downloaded from the ESA website (https://www.esa.int/ESA) to achieve sufficient spatial and temporal coverage of PRE. In total, 350 images (2003–2011) were used in this research.

Self-organizing map

The self-organizing map (SOM) is a widely used unsupervised NN, which can be applied to identify underlying patterns from the input data. The SOM is a competitive learning algorithm, which competes to best represent the input data without any human intervention during the learning process. SOM is

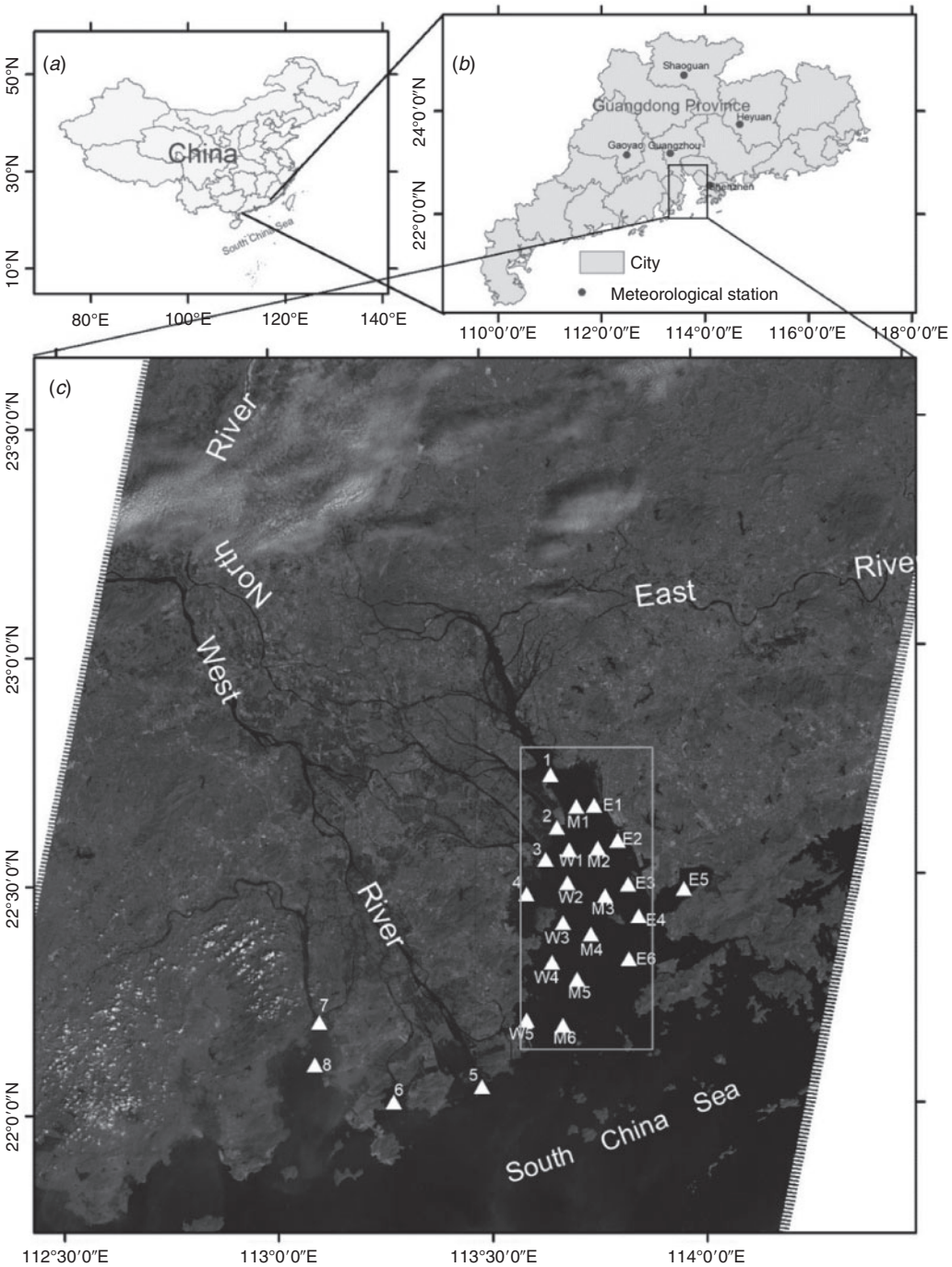

Fig. 1. (*a*) Location of the Guangdong Province in China. (*b*) Meteorological station in Guangdong Province, including the Gaoyao, Shaoguan, Guangzhou, Heyuan and Shenzhen. (*c*) Location of the Pearl River estuary in Guangdong Province, showing the Linddingyang (dashed box). Numbers on the map represent the following eight 'gates': 1, Humen; 2, Jiaomen; 3, Hongqili; 4, Hengmen; 5, Modaomen; 6, Jitimen; 7, Hutiaomen; and 8, Yamen.

different from other artificial NN (ANN) in the sense that it uses a neighbourhood function to preserve the topological properties of the input space. SOM operates in two modes, namely, training and mapping. A schematic of the training of the SOM is shown in Fig. 2. Detailed information about SOM can be found in Richardson *et al.* (2003). For all TSM images, clouds were coded as a missing value and had no influence on the analysis. The SOM has the ability to deal with missing data without *a priori* interpolation, which is a useful aspect of the SOM that is not the case for other multivariate approaches (Richardson *et al.*

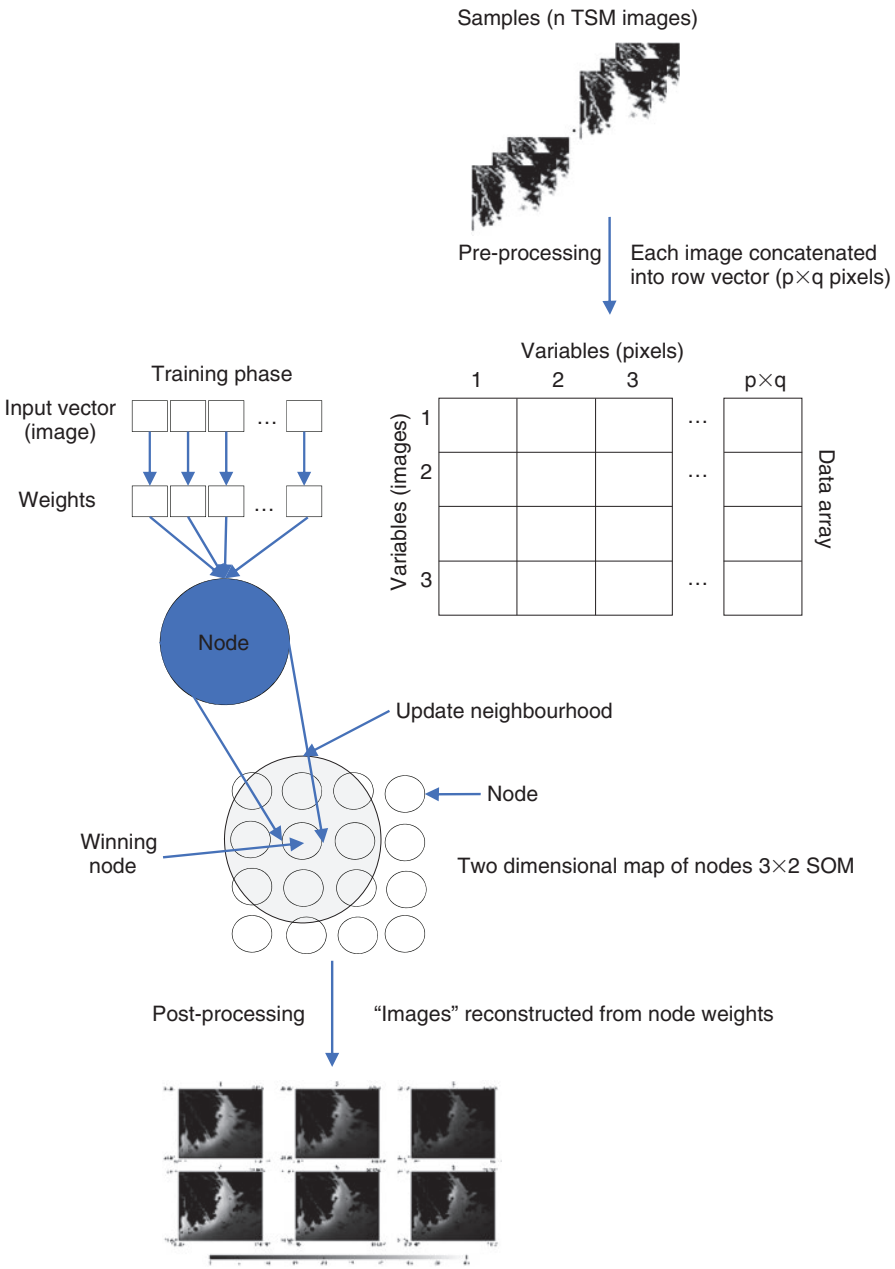

Fig. 2. A schematic depicting the implementation of the self-organising map, including pre-processing, training and post-processing phases (Richardson *et al.* 2003).

2003). In the present study, a 3 × 2 SOM was used to extract spatial-distribution patterns of TSM concentration from 350 TSM images. To apply the SOM to satellite images, some pre- and post-processing of the data is necessary. Each TSM image (480 × 400 pixels) was transformed into a single row vector by concatenating each row in the image. The final input matrix consisted of 192 000 columns (pixels) × 350 rows. After the SOM was performed, the final weights for each node were reformed into two-dimensional images (Fig. 2). Finally, the relative frequency of occurrence of each spatial-distribution pattern was calculated and was shown in Fig. 2. The SOM algorithm was implemented using the *Somoclu* package (see https://somoclu.readthedocs.io/en/stable/index.html, accessed 11 February 2019) and Python 3 programming language (see https://www.python.org/, accessed 11 February 2019). These calculations were all completed using an open-source software Anaconda3 (see https://www.anaconda.com, accessed 11 February 2019).

Meteorological data

Meteorological data in the study area were used because of the probable influence on the spatial and temporal variability of TSM concentration. Meteorological data, including average monthly rainfall (mm) and average monthly wind speed (m s^{-1})

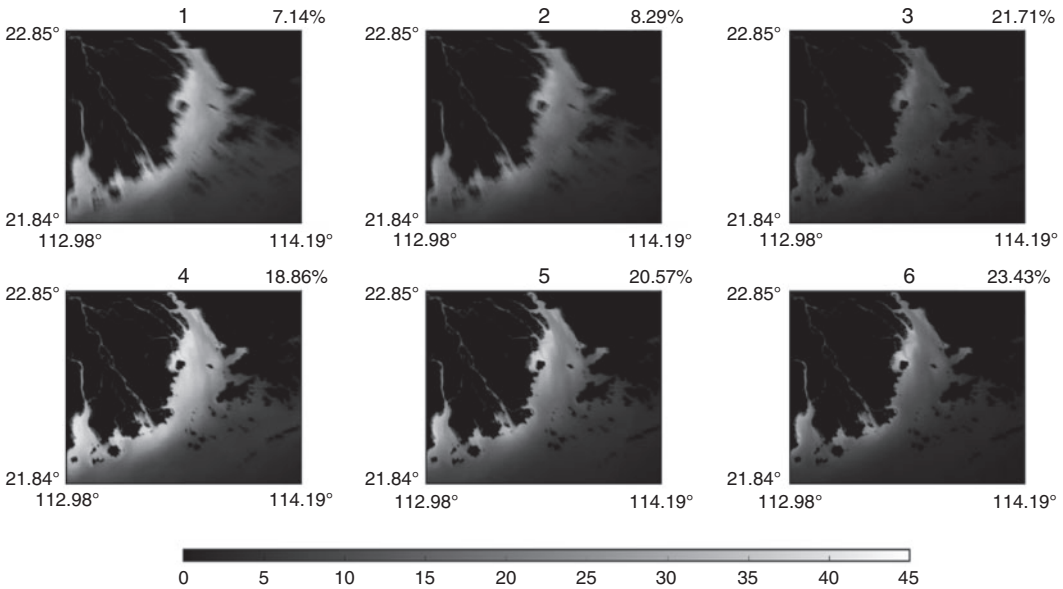

Fig. 3. A 3 × 2 self-organising map of 350 total suspended matter (TSM) images in the Pearl River estuary region. The following training parameters were used: initial training consisted of 1000 iterations, the initial learning rate was 0.2 and the learning rate in the final epoch was 0.05, and the initial radius was 5 and the radius in the final epoch was 0. The relative frequency of each spatial pattern is shown in the top right of each pattern. The unit of TSM concentration is grams per cubic metre. The black areas in each subplot are land.

from 2003 to 2011, were obtained from the China Meteorological Data Sharing Service System (see http://data.cma.cn/, accessed 11 February 2019). We chose five meteorological stations, including Gaoyao, Heyuan, Shaoguan, Guangzhou and Shenzhen (Fig. 1), to represent meteorological conditions for Xijiang, Beijiang and Dongjiang.

Statistical analysis

Annual mean TSM concentrations at each sample site during the period from 2003 to 2011 were used to calculate the maximum, minimum, mean and median values, and to map the box-plot figures. Two-sample Student's *t*-test was performed using Python to see the significance of spatial variation in TSM concentration for the eight outlets and the Lingdingyang Bay. The significance level was reported to be significant ($P \leq 0.05$) or not significant ($P > 0.05$).

Results

Spatial-distribution patterns of TSM in the PRE

Spatial-distribution patterns of TSM concentration in the PRE were identified by SOM from 350 TSM images for the time frame from May 2003 to November 2011. A 3 × 2 SOM of 350 TSM images is shown in Fig. 3. There is a continuum of change across the SOM array, with high TSM values on the western shore, and low TSM values on the eastern shore and off the PRE. The relative frequency of occurrence of each pattern is also shown in Fig. 3, indicating that all SOM output patterns exist in the input data. The most common synoptic TSM pattern, occurring in 23.43% of the images, was Node 6. The highest synoptic TSM pattern, occurring in 18.86% of the images, was Node 4. It can be found that the high TSM concentration in the PRE is characterised in coastal areas and decreases gradually from coastal waters to offshore waters. Although patterns on the left and right in the SOM array have a big difference, these patterns obtained a similar spatial-distribution characteristic of TSM concentration. Each pattern presented a strip distribution from north-east to south-west and the values of TSM were decreasing regularly from north-west to south-west. The patterns (i.e. Nodes 1, 4 and 5) represent the spatial distribution of a high TSM concentration that comes from the stratification of the input data (TSM images in this study) with high TSM values mainly distributed in the wet season. By contrast, patterns (i.e. Nodes 2, 3 and 6 in Fig. 3) represent spatial distribution of a low TSM concentration that comes from the stratification of the input data with low TSM values mainly distributed in the dry season. These findings are consistent with local circumstances and previous researches (Liu *et al.* 2009; Fu *et al.* 2016), which also confirmed that SOM is a powerful tool for identifying spatial patterns.

Spatial and temporal variations of TSM concentration

Spatial variation

Box-plots (also called box and whisker plots) of TSM concentration in the eight outlets, Xitan, Zhongtan and Dongtan during the period from 2003 to 2011 were examined (Fig. 4). The red triangle represents the location of the mean annual value at each sample point during the period 2003–2011. Individual points with values outside these limits are plotted with asterisks. Box-plot provides a visual impression of the location and shape of the underlying distributions. For example, box-plot with long whiskers at the top of the box, such as TSM concentration in Yamen, point to skewed underlying distribution towards a high concentration. By inspecting these plots, it is possible to

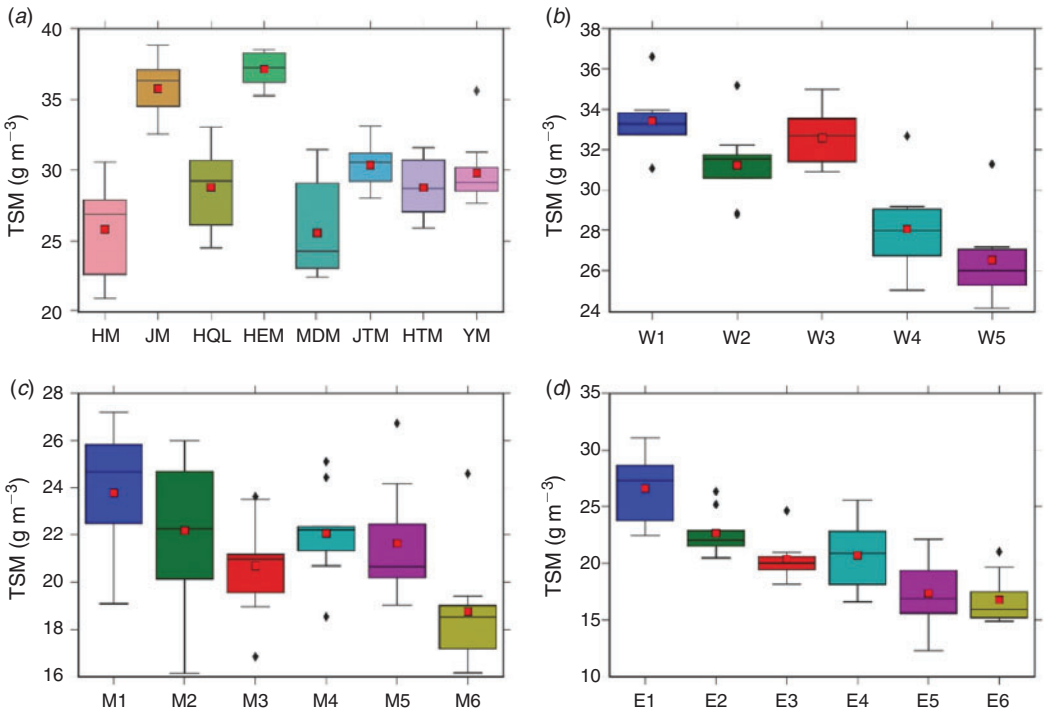

Fig. 4. Box plot of annual mean total suspended matter (TSM) concentration in all selected sample points during the period from 2003 to 2011. Annual mean value of TSM concentration at each sample point is the mean value for annual average TSM of each year, from 2003 to 2011.

perceive differences among the selected sample points. There was no significant spatial variation between Jiaomen and Hengmen ($P = 0.097$, *t*-test), whereas significant spatial variations were observed between Jiaomen and Hengmen with other six outlets ($P < 0.0001$, *t*-test; Fig. 4*a*). Among the eight outlets, the average TSM concentration was highest in Hengmen (Fig. 4*a*) because this site receives much more suspended sediment from terrestrial inputs (i.e. agriculture runoff, urban surface runoff, deforestation and water discharge; Dai *et al.* 2008), which was mainly collected from the runoff from the Dongjiang and the Beijiang as well as a portion of the Xijiang (Zhai *et al.* 2005). The average TSM concentration was lowest in Modaomen, because this is mainly due to the construction of dams (Longtan Dam) in the upstream (Wu *et al.* 2016), which reduces the sediment flowing into the Modaomen estuary (Wu *et al.* 2014). It can be found that the average TSM concentration in Humen was almost the same as Modaomen. Followed by Hengmen, the average TSM concentration of Jiaomen was the second largest. There was little difference in average TSM concentrations for the other four outlets during the period of 2003–2011 (Fig. 4*a*).

The samples located in the Lingdingyang Bay showed a large variation (Fig. 4*b–d*), with the highest average values being observed near the outlet of Jiaomen and Humen (W1, M1 and E1), and the lowest average values being found in the far offshore regions (W5, M6 and E5). Moreover, the average TSM concentration of Xitan was higher than those of Zhongtan and Dongtan (Fig. 4*b–d*), which is consistent with previous studies (Zhang *et al.* 2010; Zhu *et al.* 2015). At $\alpha = 0.05$ level, there was a statistically significance between W1, W2 and W3, and W4 and W5. Additionally, significant spatial variation in the statistical significance level was observed between M1, M2, M4 and M5, and M6 ($P < 0.05$, *t*-test; Fig. 4*c*). There was a significant spatial variation between E1, E2, E3 and E4, and E5 and E6 ($P < 0.05$, *t*-test; Fig. 4*d*).

Annual variation

Annual mean TSM concentration in all selected sample points and in the whole PRE during the period from 2003 to 2011 is shown in Fig. 5 and 6 respectively. Annual average of TSM concentration shows a large variation in the PRE within the time frame from 2003 to 2011. Overall, the highest values were found in 2003, whereas the lowest values varied among different sample points during the period from 2003 to 2011 (Fig. 5). As for the whole PRE, the distribution of the lowest TSM concentration occurred in the year of 2004 (Fig. 6). The spatial distribution of TSM concentration in each year presented significant differences because of the variation in environment conditions (e.g. precipitation and surface runoff). However, the TSM concentration in the PRE showed the same spatial-distribution characteristics; namely, the highest values occurred in the coastal waters and the lowest values in the offshore waters. The temporal variation in the TSM concentration was significant for Humen, Hongqili, Modaomen, Jitimen, Hutiaomen and Yamen during the period from 2003 to 2011, whereas Jiaomen and Hengmen were relatively homogenous (Fig. 5*a*, *b*). It is worth noting that the inter-annual variation of TSM concentration in Humen, Hongqili and Modaomen is large, with Humen and Hongqili

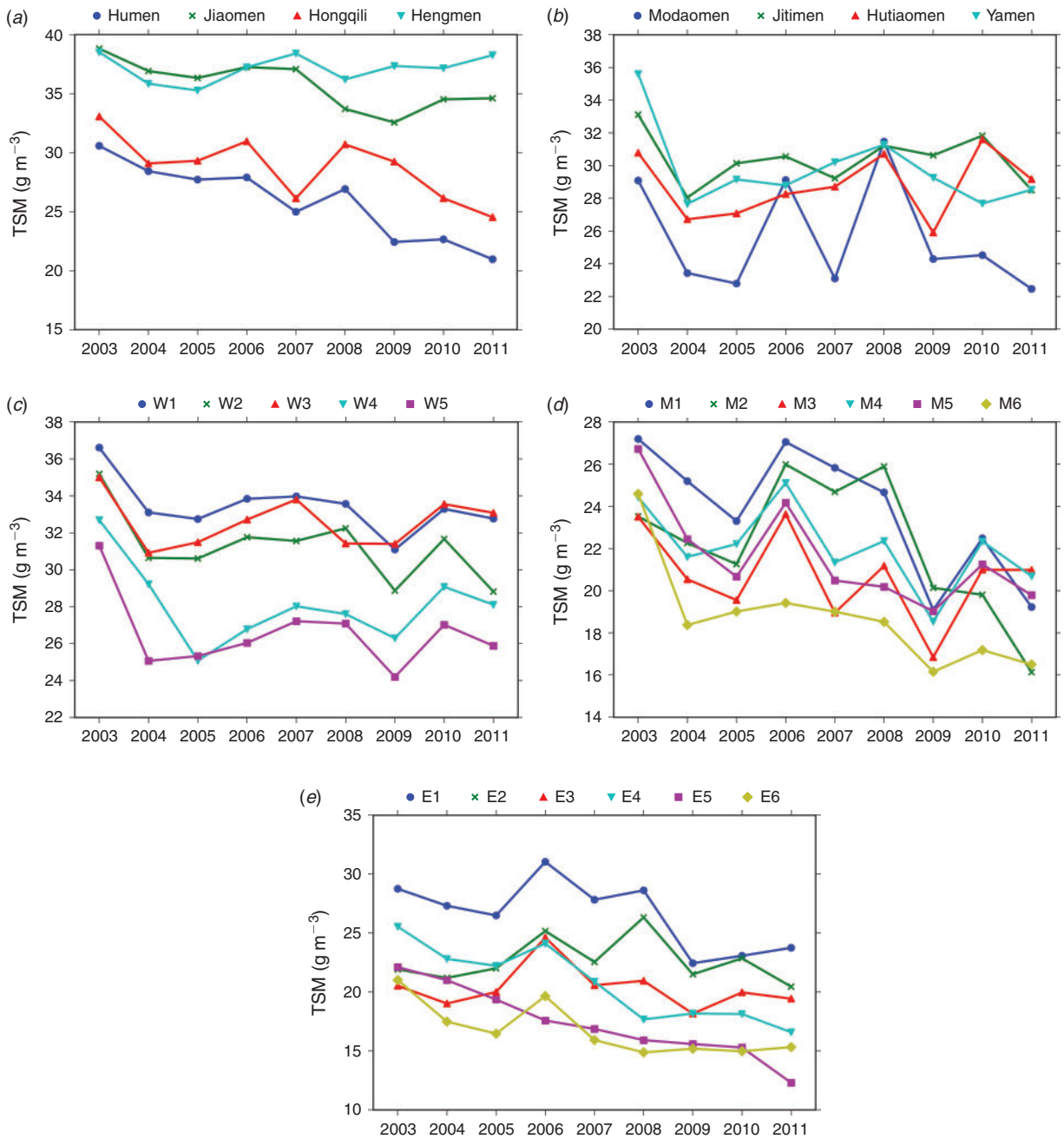

Fig. 5. Annual mean total suspended matter (TSM) concentration in all selected sample points. Annual mean value of TSM concentration is the mean value for all TSM product images each year, from 2003 to 2011.

experiencing a similar decreasing trend. However, TSM concentration in Humen and Hongqili decreased sharply from 2006 to 2007 and increased sharply from 2007 to 2008. This may be explained by the fact that the autumn-rainfall distribution showed a typical feature of more than normal in North China and less than normal in South China in 2007, especially in September and October (Jia *et al.* 2008), which was probably due to abnormally weak cold air in the far-northern part of the region (Deng *et al.* 2017).

Modaomen experienced five markedly different variations from 2003 to 2011, namely (1) a decrease from 2003 to 2005, (2) a sharp increase from 2005 to 2006, (3) a sharp decrease from 2006 to 2007, (4) a sharp increase from 2007 to 2008 and (5) a decrease from 2008 to 2011. This may have resulted from agricultural runoff, strong tidal currents and the construction of large dams in the upstream of Xijiang (Fig. 5*b*).

For the annual variation of TSM concentration in Xitan region (Fig. 5*c*), the TSM concentration decreased dramatically

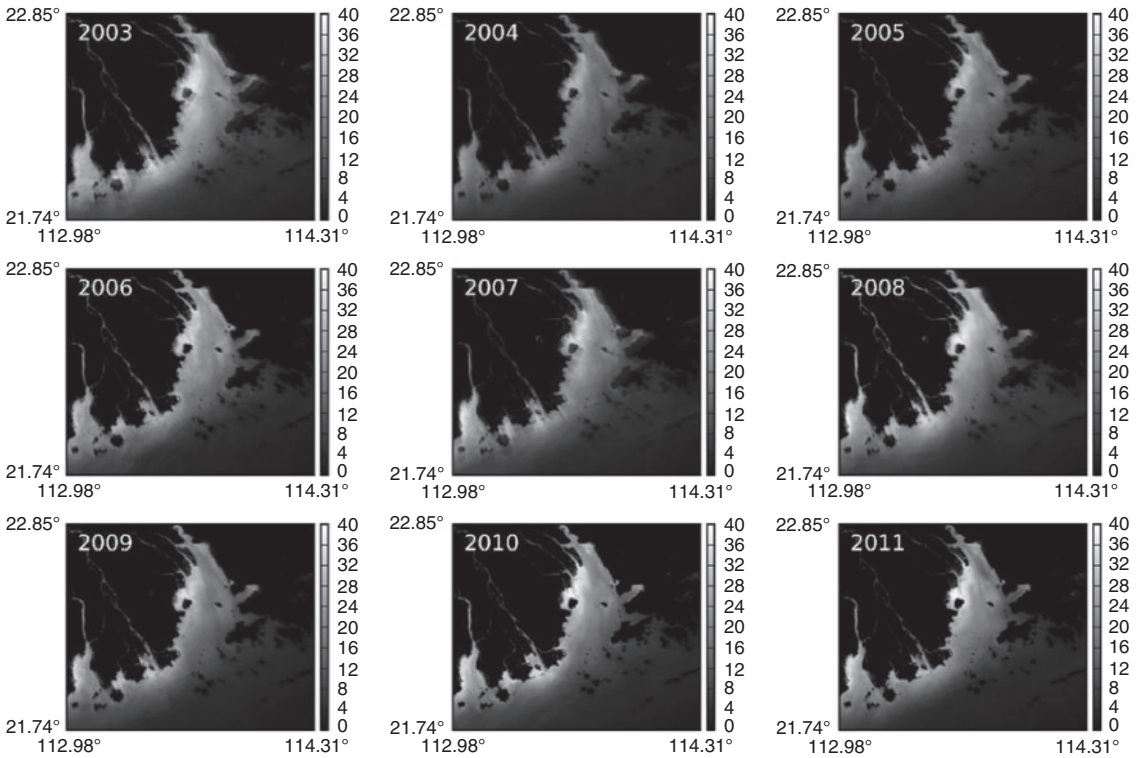

Fig. 6. Annual mean total suspended matter (TSM) concentration in the Pearl River estuary. Annual mean value of TSM is the mean value for all TSM images each year, from 2003 to 2011. The unit of the TSM concentration is grams per cubic metre. The black areas in each subplot are land.

from 2003 to 2004, and then increased gradually from 2004 to 2008, and decreased sharply from 2008 to 2009, and increased sharply from 2009 to 2010 and finally decreased from 2010 to 2011. These results can also be observed from the long-term annual average TSM concentration in the whole PRE (Fig. 6). This is because suspended sediment in Xitan is mainly influenced by terrestrial input. Compared with Xitan, the TSM concentration of Zhongtan varied greatly during the period from 2003 to 2011 (Fig. 5*d*, 6). This may be related to topography and meteorological factors (e.g. precipitation and wind speed). For the annual mean TSM concentration of Dongtan, TSM concentration of E5 decreased gradually from 2003 to 2011, whereas that of the other five sites varied among different years, especially for the year of 2006, which was mainly due to a large amount of terrestrial sediment flowing into the Lingdingyang Bay and spreading to the Dongtan (Fig. 5*e*, 6).

Monthly and seasonal variation

Monthly mean TSM concentration in all selected sample points and in the whole PRE from January to December is shown in Fig. 7 and 8 respectively. Seasonal mean TSM concentrations in the whole PRE are presented in Fig. 9. For most of the sample points, monthly mean TSM concentration showed a clear-cut seasonal effect, except for Jiaomen, Hongqili and Hengmen. The monthly mean TSM concentration was highest approximately July and December, whereas the lowest concentration was observed approximately May and August (Fig. 7), which is attributed to the seasonality effect. The effect of season on TSM concentration can be expressed as a 'W' distribution. A decrease in the TSM concentration from January to April was followed by an increase from April to July, and then a decrease from July to September, which was followed by an increase from September to December. In other words, the monthly mean TSM concentration for most of the sample points (except for Jiaomen, Hongqili and Hengmen; Fig. 7*a*) was higher in summer (June–August) and winter (December–February) than in spring (April–May) and autumn (September–November). This may have resulted from soil erosion, stream inputs, surface runoff and meteorological conditions (south-west monsoon in summer and north-east monsoon in winter) and tidal currents, which carry more suspended sediment into the PRE and facilitate suspended-particle pumping from deep water during summer and winter. It should be noted that the trend of the Jiaomen, Hongqili and Hengmen was different from that of the other sample points. Inversely, there was a peak in April. In addition, the lowest values in eight outlets (except for Jiaomen, Hongqili and Hengmen) occurred in April, whereas the lowest value was observed in May for sample points in Lingdingyang Bay. This may be related to the lagging effect of sediment transport and tidal cycle. As shown in Fig. 8, the distribution of TSM concentration in the PRE shows a significant seasonal variation. Specially, the monthly distribution of TSM concentration increased from May to July, and then decreased from July to August, and then increased from August to December, and

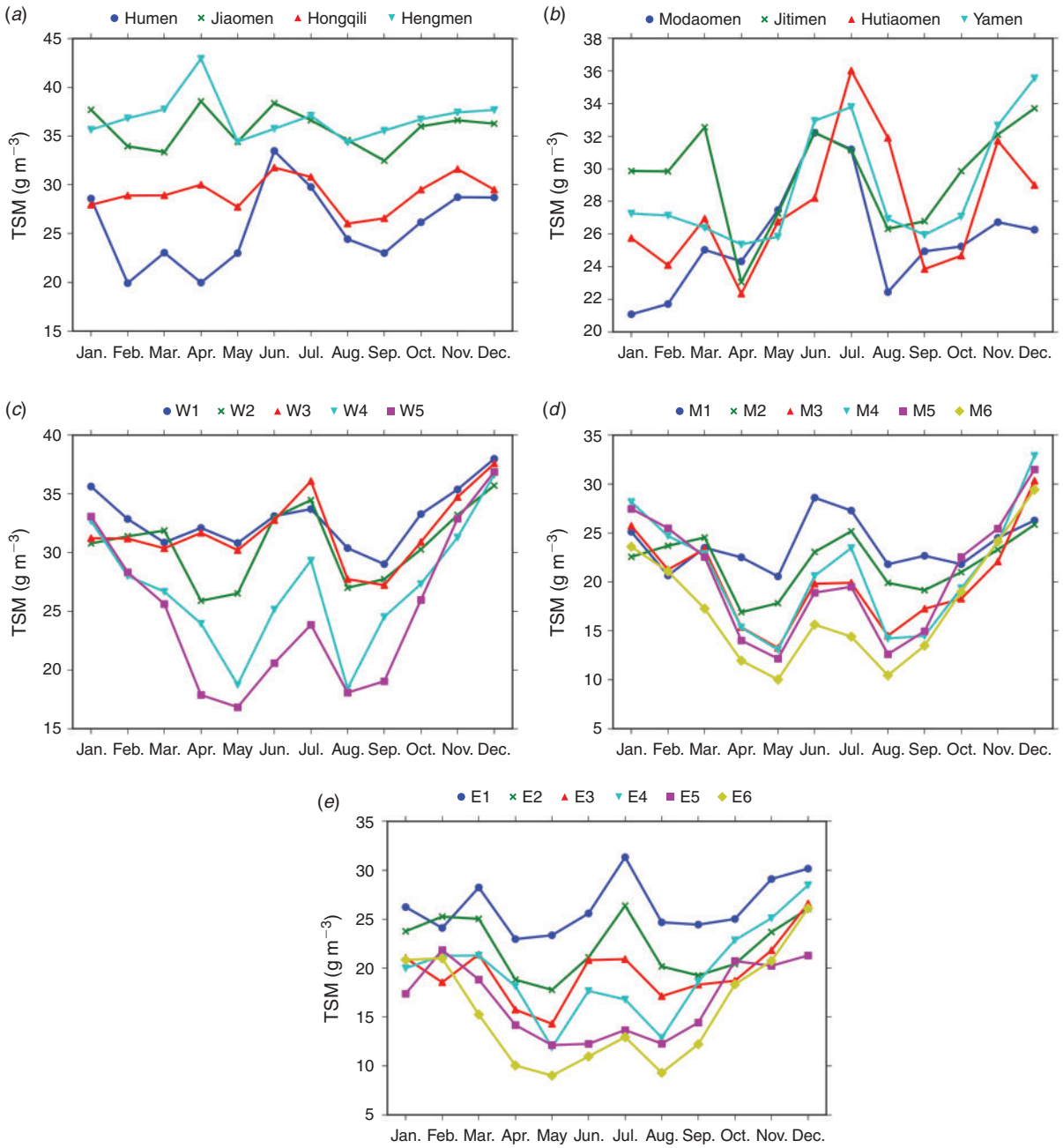

Fig. 7. Monthly mean total suspended matter (TSM) concentration in all selected sample points. Monthly mean value of TSM concentration is the mean value of for all TSM product images each month, from May 2003 to November 2011.

finally decreased from December to April. In the process of seasonal variation, the highest value was reached in July or December (Fig. 8). Overall, TSM concentration exhibited typical seasonal variability over PRE, with significantly higher values occurring in summer, autumn and winter than in spring (Fig. 9).

Discussion

The spatial-distribution patterns of TSM were extracted by SOM. This representation not only highlighted the spatial-distribution characteristics, but also showed its seasonal patterns. The Nodes 1 and 4 represent the distribution of TSM concentration in summer (July), autumn (September, October and November) and winter (December), whereas the Nodes 2, 3, 5 and 6 represent the rest of the months (Fig. 2, 7, 8). The west of the Lingdingyang Bay presents a high TSM concentration (Fig. 2; Nodes 1 and 4) because this region not only receives part of sediment and water discharge from Humen, but also receives a large amount of silt from Jiaomen, Hongqili and Hengmen rivers, which accounts for ~50% of the total sediment load from the PR (Luo *et al.* 2007). The west bank of the Huangmaohai

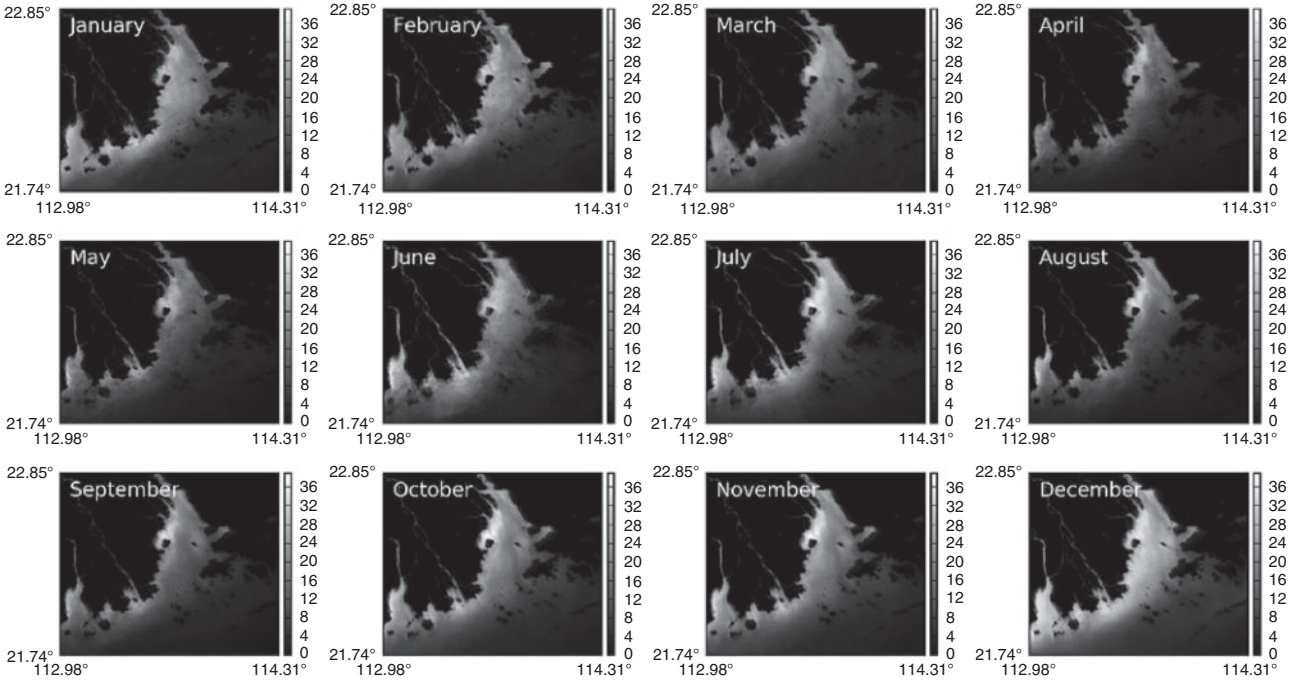

Fig. 8. Monthly mean total suspended matter (TSM) concentration in the Pearl River estuary. Monthly mean value of TSM is the mean value for all images each month, from 2003 to 2011. The unit of the TSM concentration is grams per cubic metre. The black areas in each subplot are land.

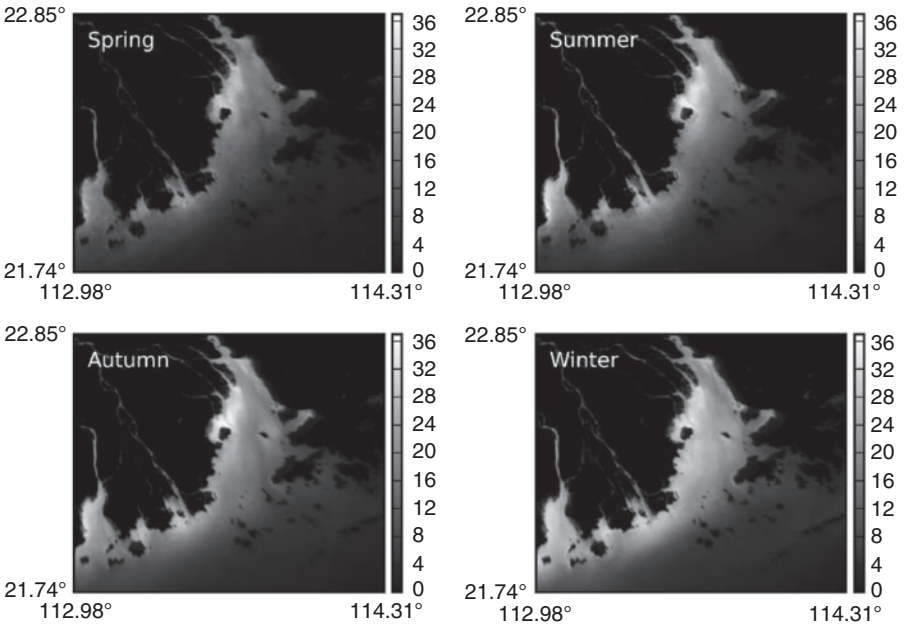

Fig. 9. Seasonal mean total suspended matter (TSM) concentration in the Pearl River estuary. Seasonal mean value of TSM concentration is the mean value for all images each season, from 2002 to 2011. The unit of the TSM concentration is grams per cubic metre. The black areas in each subplot are land.

also presented a high TSM concentration (Fig. 2, Nodes 1 and 4). This may be from the combined pressure of strong tidal currents and waves (Zhu *et al.* 2015), because the west bank is mainly affected by the north-easterly monsoon in winter. Moreover, the high TSM concentration of Modaomen is mainly affected by the large discharge of water and sediment from the Xijiang (Wu *et al.* 2016), which occupies ~78% of the total sediment load and water discharge of PR (Zhu *et al.* 2015). In the east of

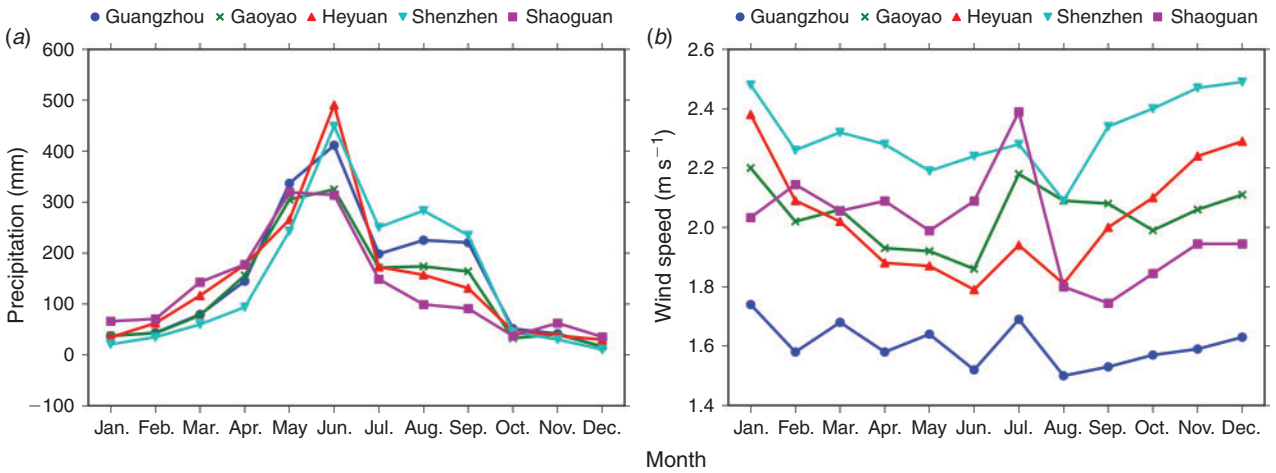

Fig. 10. Monthly average precipitation (mm) and wind speed (m s^{-1}) in Guangzhou, Gaoyao, Heyuan, Shenzhen and Shaoguan, from January 2003 to December 2011.

Lingdingyang Bay, Dongtan receives only a portion of sediment and runoff from Humen. Thus, low TSM concentration occurs in Dongtan.

During the period from 1954 to 2008, the sediment load from the PR basin carried into the SCS increased from ~69.8 Tg $year^{-1}$ (1954–1963) to 88.0 Tg $year^{-1}$ (1984–1993), and then decreased to 29.8 Tg $year^{-1}$ after the closure of the Longtan Dam (LTD) in 2006 (Wu *et al.* 2016), which is located in the upstream of the Xijiang. Inversely, water discharge from 1954 to 2008 remained relatively stable. Large variation of TSM was observed in Modaomen (Fig. 4*b*). The TSM concentration in Modaomen sharply decreased from 2003 to 2005, reaching the lowest point in 2005. This is because much of the river sediment load was trapped by reservoirs after 1994 (Wu *et al.* 2012). The effect of dams on sediment load studied by Latrubesse *et al.* (2017) demonstrated that dams can cause an ~20% decrease in the mean surface suspended-sediment concentration of the Madeira River. During the period from 2005 to 2006, TSM concentration dramatically increased, which was mainly due to the extreme weather (EI Niño). The EI Niño occurred during 2006–2007. In China, EI Niño can easily lead to warm winter (Jia *et al.* 2008). Thus, there are rainstorms and floods in the south and high temperatures and drought in the north.

In 2007, the TSM concentration in Modaomen decreased mainly because of the completion of the LTD in the PR (Dai *et al.* 2008; Wu *et al.* 2014, 2016). After the LTD began its operation in 2006, the sediment load fell from 85.9 Tg $year^{-1}$ in the 1980s and 1990s, to 29.2 Tg $year^{-1}$ from 2006 to 2011, and ~66% of the sediment load was deposited in the reservoirs (Wu *et al.* 2016). Many reservoirs have been constructed along the PR for flood control and power generation since the 1990s, and the total storage capacity had reached 621 km^3 by 2006 in the PR (Wu *et al.* 2016). The variation of TSM in Modaomen can tell us that human activities can greatly influence the spatial and temporal variation of the TSM concentration, which can effectively control the sediment delivery from the PR to PRE. After 2007, an abnormal change in the annual TSM concentration may have been from reservoir cleaning sludge (i.e. for 2008). It is worth noting that the sample points in the Lingdingyang Bay off the Humen, i.e. W1, M6 and E5, are showing a decreasing trend in TSM from 2003 to 2006, which indicates that sediment supply from terrestrial input decreased over the period of 2003–2011. In addition, soil erosion has been controlled effectively because of the implementation of different levels of water and soil conservation since the 1980s (Dai *et al.* 2008). Previous studies have shown that the subaqueous delta in Lingdingyang Bay has experienced sediment starvation and the accretion rate has decreased from 17 to 1.6 mm $year^{-1}$ (Wu *et al.* 2016). Most importantly, the decrease of the accretion rate has been more rapid than the decline in river sediment over the same period (Wu *et al.* 2016). Thus, the subaqueous delta in Lingdingyang Bay may undergo significant changes in the future.

Annual average TSM concentration decreased significantly for most of sample points in 2007 (Fig. 4), which was probably due to the effects of the La Niña event on autumn rainfall anomalies in China in 2007. Owing to abnormally weak cold air in the far-northern part of the region, the autumn-rainfall distribution showed a typical feature of the rainfall being higher than normal in northern China and lower than normal in southern China, especially in September and October (Jia *et al.* 2008). The abnormal lack of precipitation may have jointly contributed to the annual variation in 2007. Therefore, we can infer that extreme climate events (e.g. EI Niño and La Niña) may have a great effect on spatial and temporal variation of TSM concentration.

Seasonal differences in sediment and surface runoff significantly influenced the spatial distribution of TSM concentration in the PRE (Wu *et al.* 2014, 2016). Especially, in the wet season (April–September; Fig. 10*a*), a large amount of agricultural runoff and surface runoff carried a lot of sediment, which flowed into the three major tributaries (Xijiang, Beijiang and Dongjiang), and eventually through the eight gates into the SCS. The studies of Zhu *et al.* (2015) demonstrated that there is a positive relationship between sediment and water discharge and the distribution of high sediment region in the PRE. In the dry season (October–March), especially in winter, the distribution of high TSM concentration in the west of the Lingdingyang Bay

was mainly influenced by the combined pressure of strong tidal currents and the south-east monsoon (Fig. 10*b*). The fluctuation of tide and the effects of wind speed directly influence transport, sedimentation and resuspension of the sediment, which influence the distribution of TSM concentration in the PRE. This is the reason why monthly mean TSM concentration presents a 'W' distribution (Fig. 5).

Conclusions

In this study, spatial-distribution patterns of TSM concentration in the PRE were first identified by SOM from 350 MERIS FR level-2 TSM images from 2003 to 2011. The temporal and spatial variations of TSM concentration were investigated on the basis of the analysis of samples extracted from eight gates and Lingdingyang Bay. The spatial-distribution patterns of TSM in the PRE demonstrated that SOM algorithm cannot only identify spatial variation, but can also identify temporal variation (seasonality patterns). The spatial characteristics of TSM in the PRE can be summarised as follows: high values in the west and north and low values in the east and south. Seasonal patterns of TSM existed in eight gates and the Lingdingyang Bay, which presented a typical 'W' distribution in the monthly mean TSM concentration. The sources of suspended sediment and runoff in the Lingdingyang Bay are mainly controlled by terrestrial inputs. Modaomen experienced a great variation in the TSM during the period of 2003–2011 as a result of the human activities (construction of dams). Sediment resuspension influenced by the combined pressure of tidal currents and wind speed is another important factor that influences the distribution of TSM during winter. In addition, extreme climate events may (e.g. EI Niño and La Niña) have a great effect on spatial and temporal variation in TSM concentration. These results could provide a new insight for better understanding the dynamics of TSM concentration in the PRE and the effect of soil and water conservation measures in the upstream of PR.

Conflicts of interest

The authors declare that they have no conflicts of interest.

Declaration of funding

This research did not receive any specific funding.

Acknowledgements

This study was partially supported by the China National Key Technology R&D Program (2012BAH32B03), China National 863 Program (2006AA06A306) and Guangdong Natural Science Foundation (2017A030310D05). This is contribution number IS-2584 from the Guangzhou Institute of Geochemistry, Chinese Academy of Sciences, and SKLOGA201603A from the State Key Laboratory of Organic Geochemistry.

References

Alikas, K., and Reinart, A. (2008). Validation of the MERIS products on large European lakes: Peipsi, Vänern and Vättern. *Hydrobiologia* **599**, 161–168. doi:10.1007/S10750-007-9212-0

Chen, S.-L., Zhang, G.-A., Yang, S.-L., and Shi, J. Z. (2006). Temporal variations of fine suspended sediment concentration in the Changjiang River estuary and adjacent coastal waters, China. *Journal of Hydrology* **331**, 137–145. doi:10.1016/J.JHYDROL.2006.05.013

Chen, S., Han, L., Chen, X., Li, D., Sun, L., and Li, Y. (2015). Estimating wide range total suspended solids concentrations from MODIS 250-m imageries: an improved method. *ISPRS Journal of Photogrammetry and Remote Sensing* **99**, 58–69. doi:10.1016/J.ISPRSJPRS.2014.10.006

Chen, F., Wu, G., Wang, J., He, J., and Wang, Y. (2016). A MODIS-based retrieval model of suspended particulate matter concentration for the two largest freshwater lakes in China. *Sustainability* **8**, 832–846. doi:10.3390/SU8080832

Cheng, C., Wei, Y., Xu, J., and Yuan, Z. (2013). Remote sensing estimation of chlorophyll-*a* and suspended sediment concentration in turbid water based on spectral separation. *Optik* **124**, 6815–6819. doi:10.1016/J.IJLEO.2013.05.078

Dai, S. B., Yang, S. L., and Cai, A. M. (2008). Impacts of dams on the sediment flux of the Pearl River, southern China. *Catena* **76**, 36–43. doi:10.1016/J.CATENA.2008.08.004

Deng, Y., Zhang, Y., Li, D., Shi, K., and Zhang, Y. (2017). Temporal and spatial dynamics of phytoplankton primary production in Lake Taihu derived from MODIS Data. *Remote Sensing* **9**, 195. doi:10.3390/RS9030195

Doerffer, R., and Schiller, H. (2007). The MERIS Case 2 water algorithm. *International Journal of Remote Sensing* **28**, 517–535. doi:10.1080/01431160600821127

Downing-Kunz, M. A., and Schoellhamer, D. H. (2013). Seasonal variations in suspended-sediment dynamics in the tidal reach of an estuarine tributary. *Marine Geology* **345**, 314–326. doi:10.1016/J.MARGEO.2013.03.005

Duan, W., Takara, K., He, B., Luo, P., Nover, D., and Yamashiki, Y. (2013). Spatial and temporal trends in estimates of nutrient and suspended sediment loads in the Ishikari River, Japan, 1985 to 2010. *The Science of the Total Environment* **461–462**, 499–508. doi:10.1016/J.SCITOTENV.2013.05.022

Fu, D., Luan, H., Liu, D., Zhang, Y., and Ding, Y. (2016). Analysis of suspended sediment concentration remote sensing models in winter and spring in the Pearl River estuary. *Marine Environmental Science* **35**, 600–604.

González Vilas, L., Spyrakos, E., and Torres Palenzuela, J. M. (2011). Neural network estimation of chlorophyll a from MERIS full resolution data for the coastal waters of Galician rias (NW Spain). *Remote Sensing of Environment* **115**, 524–535. doi:10.1016/J.RSE.2010.09.021

Jia, X., Zhang, P., Chen, L., Gao, H., Zhu, Y., Li, W., and Han, R. (2008). Causality analysis of autumn rainfall anomalies in China in 2007. *Meteorological Monographs* **34**, 86–94.

Kratzer, S., Brockmann, C., and Moore, G. (2008). Using MERIS full resolution data to monitor coastal waters – a case study from Himmerfjärden, a fjord-like bay in the northwestern Baltic Sea. *Remote Sensing of Environment* **112**, 2284–2300. doi:10.1016/J.RSE.2007.10.006

Latrubesse, E. M., Arima, E. Y., Dunne, T., Park, E., Baker, V. R., d'Horta, F. M., Wight, C., Wittmann, F., Zuanon, J., Baker, P. A., Ribas, C. C., Norgaard, R. B., Filizola, N., Ansar, A., Flyvbjerg, B., and Stevaux, J. C. (2017). Damming the rivers of the Amazon basin. *Nature* **546**(7658), 363–369. doi:10.1038/NATURE22333

Le, C., Lehrter, J. C., Schaeffer, B. A., Hu, C., Murrell, M. C., Hagy, J. D., Greene, R. M., and Beck, M. (2016). Bio-optical water quality dynamics observed from MERIS in Pensacola Bay, Florida. *Estuarine, Coastal and Shelf Science* **173**, 26–38. doi:10.1016/J.ECSS.2016.02.003

Li, P., Yang, S. L., Milliman, J. D., Xu, K. H., Qin, W. H., Wu, C. S., Chen, Y. P., and Shi, B. W. (2012). Spatial, temporal, and human-induced variations in suspended sediment concentration in the surface waters of the Yangtze estuary and adjacent coastal areas. *Estuaries and Coasts* **35**, 1316–1327. doi:10.1007/S12237-012-9523-X

Liang, Q., Zhang, Y., Ma, R., Loiselle, S., Li, J., and Hu, M. (2017). A MODIS-based novel method to distinguish surface cyanobacterial scums and aquatic macrophytes in Lake Taihu. *Remote Sensing* **9**, 133. doi:10.3390/RS9020133

Liu, F., Chen, C., Tang, S., and Liu, D. (2009). A piecewise algorithm for retrieval of suspended sediment concentration based on in situ spectral data by MERIS in Zhujiang River estuary. *Journal of Tropical Oceanography* **28**, 9–14.

Liu, H., He, Q., Wang, Z., Weltje, G. J., and Zhang, J. (2010). Dynamics and spatial variability of near-bottom sediment exchange in the Yangtze estuary, China. *Estuarine, Coastal and Shelf Science* **86**, 322–330. doi:10.1016/J.ECSS.2009.04.020

Lu, Z., and Gan, J. (2015). Controls of seasonal variability of phytoplankton blooms in the Pearl River estuary. *Deep-sea Research – II. Topical Studies in Oceanography* **117**, 86–96. doi:10.1016/J.DSR2.2013.12.011

Luo, X.-L., Zeng, E. Y., Ji, R.-Y., and Wang, C.-P. (2007). Effects of in-channel sand excavation on the hydrology of the Pearl River delta, China. *Journal of Hydrology* **343**, 230–239. doi:10.1016/J.JHYDROL.2007.06.019

Mao, Z., Chen, J., Pan, D., Tao, B., and Zhu, Q. (2012). A regional remote sensing algorithm for total suspended matter in the East China Sea. *Remote Sensing of Environment* **124**, 819–831. doi:10.1016/J.RSE.2012.06.014

Miller, R. L., and McKee, B. A. (2004). Using MODIS Terra 250 m imagery to map concentrations of total suspended matter in coastal waters. *Remote Sensing of Environment* **93**, 259–266. doi:10.1016/J.RSE.2004.07.012

Onderka, M., and Pekarova, P. (2008). Retrieval of suspended particulate matter concentrations in the Danube River from Landsat ETM data. *The Science of the Total Environment* **397**, 238–243. doi:10.1016/J.SCITOTENV.2008.02.044

Ouyang, T., Zhu, Z., and Kuang, Y. (2006). Assessing impact of urbanization on river water quality in the Pearl River delta economic zone, China. *Environmental Monitoring and Assessment* **120**, 313–325. doi:10.1007/S10661-005-9064-X

Restrepo, J. D., Park, E., Aquino, S., and Latrubesse, E. M. (2016). Coral reefs chronically exposed to river sediment plumes in the southwestern Caribbean: Rosario Islands, Colombia. *The Science of the Total Environment* **553**, 316–329. doi:10.1016/J.SCITOTENV.2016.02.140

Richardson, A. J., Risien, C., and Shillington, F. A. (2003). Using self-organizing maps to identify patterns in satellite imagery. *Progress in Oceanography* **59**, 223–239. doi:10.1016/J.POCEAN.2003.07.006

Robert, E., Grippa, M., Kergoat, L., Pinet, S., Gal, L., Cochonneau, G., and Martinez, J.-M. (2016). Monitoring water turbidity and surface suspended sediment concentration of the Bagre Reservoir (Burkina Faso) using MODIS and field reflectance data. *International Journal of Applied Earth Observation and Geoinformation* **52**, 243–251. doi:10.1016/J.JAG.2016.06.016

Rodríguez-Blanco, M. L., Taboada-Castro, M. M., and Taboada-Castro, M. T. (2010). Factors controlling hydro-sedimentary response during runoff events in a rural catchment in the humid Spanish zone. *Catena* **82**, 206–217. doi:10.1016/J.CATENA.2010.06.007

Schroeder, T., Schaale, M., and Fischer, J. (2007). Retrieval of atmospheric and oceanic properties from MERIS measurements: a new Case-2 water processor for BEAM. *International Journal of Remote Sensing* **28**, 5627–5632. doi:10.1080/01431160701601774

Shen, F., Verhoef, W., Zhou, Y., Salama, M. S., and Liu, X. (2010). Satellite estimates of wide-range suspended sediment concentrations in Changjiang (Yangtze) estuary using MERIS data. *Estuaries and Coasts* **33**, 1420–1429. doi:10.1007/S12237-010-9313-2

Sørensen, K., Aas, E., and Høkedal, J. (2007). Validation of MERIS water products and bio-optical relationships in the Skagerrak. *International Journal of Remote Sensing* **28**, 555–568. doi:10.1080/01431160600815566

Suif, Z., Fleifle, A., Yoshimura, C., and Saavedra, O. (2016). Spatio-temporal patterns of soil erosion and suspended sediment dynamics in the Mekong River basin. *The Science of the Total Environment* **568**, 933–945. doi:10.1016/J.SCITOTENV.2015.12.134

Sun, L., Yan, M., Cai, Q., and Fang, H. (2016). Suspended sediment dynamics at different time scales in the Loushui River, south-central China. *Catena* **136**, 152–161. doi:10.1016/J.CATENA.2015.02.014

Varol, M., Gökot, B., Bekleyen, A., and Şen, B. (2012). Spatial and temporal variations in surface water quality of the dam reservoirs in the Tigris River basin, Turkey. *Catena* **92**, 11–21. doi:10.1016/J.CATENA.2011.11.013

Wang, C., Li, W., Chen, S., Li, D., Wang, D., and Liu, J. (2018). The spatial and temporal variation of total suspended solid concentration in Pearl River estuary during 1987–2015 based on remote sensing. *The Science of the Total Environment* **618**, 1125–1138. doi:10.1016/J.SCITOTENV.2017.09.196

Wu, C. S., Yang, S. L., and Lei, Y.-p. (2012). Quantifying the anthropogenic and climatic impacts on water discharge and sediment load in the Pearl River (Zhujiang), China (1954–2009). *Journal of Hydrology* **452–453**, 190–204. doi:10.1016/J.JHYDROL.2012.05.064

Wu, C. S., Yang, S., Huang, S., and Wang, S. (2014). Multi-scale variability of water discharge and sediment load in the Pearl River during 1954–2011. *Acta Geographica Sinica* **69**, 422–432.

Wu, C. S., Yang, S., Huang, S., and Mu, J. (2016). Delta changes in the Pearl River estuary and its response to human activities (1954–2008). *Quaternary International* **392**, 147–154. doi:10.1016/J.QUAINT.2015.04.009

Xi, H., and Zhang, Y. (2011). Total suspended matter observation in the Pearl River estuary from in situ and MERIS data. *Environmental Monitoring and Assessment* **177**, 563–574. doi:10.1007/S10661-010-1657-3

Xing, Q., Lou, M., Chen, C., and Shi, P. (2013). Using in situ and satellite hyperspectral data to estimate the surface suspended sediments concentrations in the Pearl River estuary. *IEEE Journal of Selected Topics in Applied Earth Observations and Remote Sensing* **6**, 731–738. doi:10.1109/JSTARS.2013.2238659

Yu, Z., Chen, X., Zhou, B., Tian, L., Yuan, X., and Feng, L. (2012). Assessment of total suspended sediment concentrations in Poyang Lake using HJ-1A/1B CCD imagery. *Chinese Journal of Oceanology and Limnology* **30**, 295–304. doi:10.1007/S00343-012-1094-Y

Zhai, W., Dai, M., Cai, W.-J., Wang, Y., and Wang, Z. (2005). High partial pressure of CO_2 and its maintaining mechanism in a subtropical estuary: the Pearl River estuary, China. *Marine Chemistry* **93**, 21–32. doi:10.1016/J.MARCHEM.2004.07.003

Zhang, W., Xu, Z., Dong, X., and Lin, N. (2010). Analysis on characteristics of temporal and spatial variation of suspended sediment in the Lingding Bay. *Journal of Sedimentary Research* **4**, 22–28.

Zhu, F., Ou, S., Zhang, S., and Luo, K. (2015). MODIS images-based retrieval and analysis of spatial-temporal change of superficial suspended sediment concentration in the Pearl River estuary. *Journal of Sedimentary Research* **2**, 67–73.

Handling Editor: Yunlin Zhang